REVISION- 1

Formation of clinohumite ± spinel in dolomitic marbles from the Makrohar Granulite Belt, Central India: Evidence for Ti mobility during regional metamorphism

SHREYA KARMAKAR

Department of Geological Sciences, Jadavpur University, Kolkata 700032, INDIA.

shreya196@gmail.com

Corresponding author:

Shreya Karmakar

shreya196@gmail.com

Department of Geological Sciences,

Jadavpur University,

Kolkata 700032, INDIA.

ABSTRACT

The mobility of Ti, a member of high field strength elements, in metamorphic fluids is crucial to understand the recycling of commonly perceived nominally soluble elements and for mass-flux calculations during crustal processes. In this study we present evidence for large scale Ti mobility from a suite of clinohumite ± spinel bearing dolomitic marbles from Makrohar area in central India. The studied rocks dominantly contain dolomite and calcite (in subequal proportions) and subordinate amount of forsterite. It commonly develops 1-5 cm thick, laterally continuous, mostly parallel sometimes anastamosing, brown coloured clinohumite rich bands with variable spinel. Clinohumite has moderate Ti and F (TiO_2=0.55-2.88wt%; F=0.94-1.88wt%; n=32). Textural and phase equilibria modelling indicate that clinohumite grew at the expense of forsterite + dolomite under static conditions due to infiltration of F and Ti bearing extremely H_2O-rich fluids (X_{CO2}<0.03), at ~5-6 kbar pressure and ~650-700°C temperature. The Ti and F were most likely supplied by highly channelized aqueous fluids restricted within the cm-thick bands. The negative volume change of the reactions further facilitated fluid ingress. The lateral continuity of the bands over several meters across multiple outcrops indicate that Ti was mobile at meter to kilometer scale. The results are in accordance with experimental studies that solubility of Ti increases in the presence of halides, and imply that Ti may be much more mobile in metamorphic fluids during regional metamorphism, than previously anticipated.

Keywords:

clinohumite; Ti mobility; forsterite marble; textural modeling; Makrohar; Central India;

INTRODUCTION

Aqueous fluid flow is an integral part of prograde regional metamorphism (Ague 2003). Ti, the most abundant member of member of high field strength elements (HFSE, along with Zr, Hf, Nb, Ta, Th, U, REEs), is generally considered immobile during regional crustal metamorphism due to the low solubility of rutile (TiO_2) in pure H_2O (Audétat and Keppler 2005; Tropper and Manning 2005). The conservativeness and abundance of HFSEs are in turn commonly used to classify tectonic setting of igneous rocks, identify protolith of altered rocks and understand element cycling during metamorphic processes (Jiang et al. 2005 and references therein). However, there are examples from natural systems that Ti can be mobile under certain conditions and high enrichment up to even economic significance may occur (Tanis et al. 2016 and references therein). This makes it crucial to better understand conditions that affect the mobility of Ti (as a proxy for the HFSEs) during common metamorphic processes.

In this study we document a natural evidence of mobility of Ti during crustal metamorphism that led to formation of Ti-bearing clinohumite in a forsterite marble, from the Makrohar Granulite Belt, Central India. The humite group of minerals has a limited paragenesis wherein, Ti and F bearing clinohumite has been reported from very few contact or regionally metamorphosed limestones, dolomites and skarns (Jones et al. 1969; Franz and Ackermand 1980; Rice 1980; Ehlers and Hoinkes 1987; Gieré 1987; Young and Morrison 1992; Piazolo and Markl 1999; Tropper et al. 2007; Proyer et al. 2008; Fernandes and Chaves 2014; Proyer et al. 2014) with only a few reported occurrences in India (Muthuswami 1958; Bhattacharyya 1974; Satish-Kumar and Niimi 1998; Pradeepkumar and Krishnanath 2000; Chattopadhyay et al. 2009). Rarely, Ti-rich but F-poor members have been reported from mantle derived ultramafic rocks where they form due to high to ultra-high pressure metamorphism (Trommsdorff and Evans

1980; Evans and Trommsdorff 1983; Dymek et al. 1988; Scambelluri et al. 1991; Gaspar 1992; Okay 1994; Rahn and Bucher 1998; Wunder 1998; Scambelluri and Rampone 1999; Stalder and Ulmer 2001; Sánchez-Vizcaíno et al. 2005; Groppo and Compagnoni 2007; Shen et al. 2015; González-Jiménez et al. 2017; Nishio et al. 2019). The humite group of minerals, having a general formula of $nM_2SiO_4.M_{1-X}Ti_X(OH, F)_{2-2X}O_{2X}$, is essentially a hydrous olivine, with n=1, 2, 3, 4 for norbergite, chondrodite, humite and clinohumite respectively and M = Mg, Fe, Mn, Ca, Zn (Jones et al. 1969; Rice 1980). Ti thus plays a special role in the formation of humite minerals because the Ti content of olivines is generally quite low, whereas clinohumite may contain significantly higher amounts (Jones et al. 1969).

In the studied marbles from the Makrohar Granulite Belt, Central India, the formation of clinohumite, the only hydrous Ti and F bearing phase, in an otherwise Ti and F free assemblage of forsterite-calcite-dolomite, along parallel continuous bands of uniform thickness, indicate its formation due to infiltration of external fluids. Textural and thermodynamic modeling in the CMASV ($CaO-MgO-Al_2O_3-SiO_2-H_2O-CO_2$) system indicate that the presence of Ti and F in H_2O-rich fluids facilitated the formation of clinohumite, which in turn indicates that the presence of F in the H_2O-rich fluids must have enhanced Ti mobility, as solubility of Ti (or TiO_2) in pure water is very low (Audétat and Keppler 2005; Tropper and Manning 2005). The results are in agreement with experimental studies indicate that Ti is increasingly more mobile in halogen bearing aqueous fluids, particularly F, by forming soluble complexes with the F^- and Cl^- ions (Ryzhenko et al. 2006; Antignano and Manning 2008; Purtov and Kotel'nikova 2010; Rapp et al. 2010; Hayden and Manning 2011; Tanis et al. 2016).

REGIONAL GEOLOGY

The study area is a part of the Makrohar granulite belt (MGB) that belongs to the north-eastern part of the Central Indian Tectonic Zone (CITZ; Fig. 1). The CITZ is a ~1500 km long E-W to ENE-WSW trending Proterozoic orogenic belt that results from a complex collision between the Archean Southern and Northern Indian Blocks (Acharyya 2003; Roy and Prasad 2003; Bhowmik 2019) The CITZ contains several Proterozoic supracrustal belts of varied metamorphic grade, which are set in largely undifferentiated migmatitic gneisses and intruded by syn- to post-tectonic granitoids and mafic rocks (Acharyya 2003; Bhowmik 2019). The Mahakoshal supracrustal belt occurs along the northern fringe of the CITZ and the MGB occurs near the southern margin of the Mahakoshal supracrustal belt (Fig. 1).

The MGB dominantly comprises a suite of ~1.73 Ga granite gneisses containing slivers of charnockites (Sarkar et al. 1998; Acharyya 2003; Deshmukh et al. 2017). This whole package is intruded by a suite of mafic rocks (apatite-ilmenite bearing olivine norite) and late pegmatites, and overlain by a supracrustal package comprising the studied banded marbles and some metapelites (Fig. 1). The banded marbles occur as kilometer scale bands (up to a few meters thick) that are folded with NW-SE oriented axial planes (Fig. 1). The centimeter scale internal banding of the marbles is parallel to their length.

FIELD FEATURES AND PETROGRAPHY

The studied marbles are off-white to greyish white in color and show a saccharoidal appearance due to high degree of recrystallization (Fig. 2a-c). Microscopic study reveals that they dominantly comprise polygonal grains of dolomite and calcite (in subequal proportions) and subordinate amount of forsterite, showing a granoblastic fabric (Fig. 2d, e).

The marbles commonly develop 1-5 cm thick brown to brownish grey colored layers rich in

clinohumite and spinel (Fig. 2a-c). The layers are mostly parallel and laterally continuous within a single outcrop, a few meters in size (Fig. 2a). Small patches of white marble are occasionally preserved within the thick layers, and the layers anastomose around the patches (Fig. 2a).

Microscopically, **the brown layers** comprise almost entirely of recrystallized grains of clinohumite (80-90 vol%) with minor calcite (10-15 vol%), and rounded relict grains of forsterite (Fig. 2f). The contact between the host marbles and the brown clinohumite layers is quite sharp (Fig. 2a-c).

The brownish grey layers comprise of recrystallized grains of clinohumite, spinel and calcite. They are commonly zoned, with dark grey spinel-rich domains in the center usually grading into brownish grey spinel-poor fringes (Fig. 2a, c). The grey spinel-rich central domains (Fig. 2g) comprise of spinel (10-20 vol%) in addition to clinohumite (60-70 vol%) and calcite (10-20 vol%). The spinel grains commonly contain magnetite at their cores (Fig. 2h, i). The brownish grey spinel-poor fringes (Fig. 2g) comprise spinel (5-15 vol%) in addition to clinohumite (50-60 vol%) and calcite (20-30 vol%). The internal zonation has variable thickness with no discernible boundary between the spinel rich and poor domains (Fig. 2c). The brownish grey layers as a whole have fairly uniform thickness and their contact with the host marbles is also quite sharp, as marked by the abrupt absence of clinohumite. But due to the gradual decrease in spinel content, and the presence of 20-30 vol% calcite in the fringes, the contact with the host marbles may appear gradational (Fig. 2c).

MINERAL COMPOSITIONS

Chemical compositions of the minerals were determined with a CAMECA SX5 microprobe with 5 WD spectrometers at the Central Research Facility of the Indian School of Mines, Dhanbad,

India. The instrument was operated at 15kV accelerating voltage, 2-3 μm beam diameter and 15 nA current. Natural standards were used for most major elements (Si, Al, Cr, Fe, Mg, Ca, Na, K, Zn, Cl and F) except for Mn and Ti, for which synthetic standards were used. The raw data were corrected by PAP procedure (Pouchou and Pichoir 1984). Mineral abbreviations in figures and tables have been used after Whitney and Evans (2010). Representative mineral compositions are presented in supplementary Table 1. Most minerals show fairly uniform composition across the different outcrops/samples (Fig. 1). So the total numbers of analyses, the average values and the 2σ standard deviation for each oxide and cation are also indicated in Table 1. In the following section salient compositional features of the minerals in the studied rocks are described.

The *calcite* and *dolomite* have virtually end-member compositions. X_{Mg} in dolomite ranges between 0.98-0.99 (n=42; average=0.99±0.01). The *Forsterite* is extremely magnesian with X_{Mg} =0.96±0.01 and negligible TiO_2 (<0.04 wt%; n=32; Table 1).

The *Spinel* is fairly magnesian with X_{Mg}=0.89±0.03 and has insignificant Ti, Cr, Zn, and Mn with recalculated Fe^{+3} <0.05 a.p.f.u. (n=15; Table 1). The *magnetite* has virtually end member composition with Fe^{+3}/Fe^{+2}=2.14±0.12, 0.36±0.28 wt% TiO_2, and insignificant Cr and Al (n=10; Table 1; Fe^{+3} is recalculated after the scheme of Grew (2013)).

The *clinohumite* structural formulae were calculated based on 13 cations following the scheme of Jones et al. (1969). In spite of the slightly low analytical totals, the ratio of $2Si:[M_{Ti}*2n/(2n+1)]$=1.00±0.07 indicates that the measured compositions are stoichiometric (Jones et al. 1969) (Table 1). There are three possible exchange vectors in humite minerals: $FeMg_{-1}$, OHF_{-1}, and $TiO_2Mg_{-1}(F, OH)_{-2}$ (Jones et al. 1969; Rice 1980). Both $FeMg_{-1}$ and OHF_{-1} are observed with X_{Mg} =0.97±0.02, and the fluorine content ranging from 0.94-1.88 wt% with X_F=0.25±0.11 (Table 1). Clinohumite contains 1.14-2.88 wt% TiO_2 with M_{Ti}/Si=2.25±0.16 (ideal=2.25; Table 1). Ti vs. (OH + F) data presented in Fig. 3a show the efficiency of the

exchange vector $TiO_2Mg_{-1}(F, OH)_{-2}$ [or $(OH +F) = -2Ti +2/9M_{Ti}$] (Jones et al. 1969). A plot of TiO_2 vs. [MgO / (MgO + MnO + FeO)] after Rios et al. (2015) shows that clinohumite compositions from this study are similar to those from other marbles (Fig. 3b).

TEXTURAL MODELLING

Textural modeling is a powerful tool to identify if a given mineral assemblage developed in an open or closed system and helps to identify the mass balanced reactions among a set of minerals (Fisher 1989; Lang et al. 2004; Sengupta and Dasgupta 2009). Details of the textural modeling process can be found in Karmakar et al. (2017) and Chowdhury et al. (2013), and the computer program C-Space of Torres-Roldan et al. (2000) has been used for the same.

Observed textural features like recrystallized granoblastic texture and forsterite relicts within clinohumite, demonstrate that clinohumite and spinel both crystallized under static conditions, and also that clinohumite preferentially replaced forsterite. However, compositionally, forsterite in host rock is anhydrous and Ti-free whereas clinohumite is not only a hydrous mineral but also the sole phase that contains significant amounts of Ti and F. Therefore, it seems that clinohumite formation requires the presence of Ti and F bearing hydrous fluids. This then requires that the balanced chemical reaction that links the reactant and product phases must involve a number of mobile chemical species. However, though spinel is the sole aluminous phase in the system, dolomitic limestones usually contain minor to moderate amounts of clinochlore or Mg-chlorite (Rice 1977; Bucher-Nurminen 1981; Sharp and Buseck 1988; Bucher and Frey 1994; 2002) and the two Al-rich minerals chlorite and spinel commonly form at each other's expense during metamorphism (Novak and Houzar 1996; Buick et al. 1997; Tropper et al. 2003; Castelli et al. 2007; Groppo et al. 2007; Proyer et al. 2008; 2014; Rapa et al. 2017).

So, clinochlore is the likely precursor of spinel in the studied rocks, that was completely consumed.

Through textural modeling the following mass balanced reactions are obtained using the representative mineral compositions marked in Table 1 (Fig. 3c: dashed lines):

1. $28.41\ Dol + 40.0\ Fo + 7.00\ H_2O + 2.40\ SiO_2^{(aqueous)} + 6.72\ Ca^{+2} + 1.00\ Ti^{+4} + 6.00\ F^{-1}$
$= 16.74\ Cal + 10.00\ Chu + 16.41\ CO_2$ (ΔV_{SOLID}= -37.6%; V_{CHU}:V_{CAL}=5.8:1)

The mass balanced reaction for spinel formation is obtained using an end member clinochlore composition with only slight Fe such that X_{Mg}=0.98 (Fig. 3c: solid lines):

2a. $98.94\ Dol + 8.42\ Chl + 4.71\ Fe^{+2} + 1.00\ Ti^{+4} + 6.00\ F^{-1}$
$= 39.57\ Cal + 26.57\ Spl + 10.00\ Chu + 60.34\ H_2O + 70.24\ CO_2 + 6.25\ Mg^{+2}$
(ΔV_{SOLID}= -39.5%; V_{CHU}:V_{CAL}:V_{SPL}~2:1.5:1)

2b. $85.40\ Dol + 8.42\ Chl + 4.71\ Fe^{+2} + 1.00\ Ti^{+4} + 6.00\ F^{-1}$
$= 30.95\ Cal + 26.57\ Spl + 10.00\ Chu + 60.34\ H_2O + 62.89\ CO_2 + 4.02\ Ca^{+2}$
(ΔV_{SOLID}= -30.7%; V_{CHU}:V_{CAL}:V_{SPL}~2:1.2:1.1)

The predicted volume ratio of the product phases roughly matches observed proportions.

PHASE RELATIONS IN THE CMASV SYSTEM

Clinohumite being the sole hydrous phase in the rock, it not only formed from externally derived fluids, but its stability is also likely to be highly dependent on the fluid compositions (Rice 1980). As such, isothermal or isobaric phase diagram projections as a function of the fluid composition are a useful tool for interpreting the genetic history of such fluid-influenced assemblages (Connolly and Trommsdorff 1991). Thus topology of the clinohumite-bearing assemblages have been computed and discussed qualitatively in isothermal pressure vs. X_{CO2} (iT-P-X_{CO2}) and

isobaric temperature vs. X_{CO2} (iP-T-X_{CO2}) spaces using the computer program PERPLEX_6.8.0 (Connolly 2005; 2009). The iT-P-X_{CO2} diagram (Fig. 4a-b) has been calculated at T=600°C, and the iP-T-X_{CO2} (Fig. 4c-d) diagram was calculated separately at P=5kbar and P=6kbar, but since no significant change in topology is observed, only one figure has been presented. The reasons for selecting the iT=600°C and iP=5-6 kbar values have discussed later. However, as the influence of the key metamorphic variables P and T may get obscured in isothermal or isobaric phase diagram projections, a petrogenetic grid was also computed in mixed fluid-P-T space (Fig. 4e-f) at fixed X_{CO2}=0.13, based on the The iT-P-X_{CO2} and the iP-T-X_{CO2} diagrams.

The reaction topologies were computed using the internally consistent thermodynamic data set and equation of state for H_2O-CO_2 fluid of Holland and Powell (1998), updated in 2004. Calculations were done in the simplified six-component system CaO-MgO-Al_2O_3-SiO_2-H_2O-CO_2 (CMASV; Fig. 4). The following solid end-members were considered: calcite, dolomite, forsterite, spinel, clinohumite (Mg-OH: $Mg_9Si_4O_{16}(OH)_2$), clinochlore, brucite, periclase, antigorite, diopside, tremolite; along with binary H_2O-CO_2 fluid (Connolly and Trommsdorff 1991)3. The presence of non-CMASH components (e.g., Fe^{+2} in forsterite, spinel) expands the stability fields of the minerals that accommodate these elements by reducing the activity of the CMASH-end members. Specifically, OH-clinohumite is metastable in natural assemblages and presence of small amounts of F and Ti renders it stable in H_2O-rich fluids (Rice 1980; Grützner et al. 2017). So, in order to account for the effects of non-CMASH components, computations are done after reducing the activity of the CMASH-end members using the measured compositions of the solid-solution phases (marked with * in Fig.4; aSpl=0.83, aFo=0.94, Table 1). The activities of spinel and forsterite were obtained using the computer program AX (Tim Holland and Powell 2015). However, for the humite group of minerals, while Duffy and Greenwood

(Duffy and Greenwood 1979) have shown that they exhibit non-ideal OH-F solution behavior, activity-composition relationships for the remaining two substitutions [$FeMg_{-1}$ and $TiO_2Mg_{-1}(F,OH)_{-2}$] are not completely defined. Also, in the internally consistent database, thermodynamic data are available only for the $Mg_9Si_4O_{16}(OH)_2$ end member (derived from the experiments of Duffy and Greenwood (1979) and discussed in Pawley (2000)). So, following Sánchez-Vizcaíno et al. (2005) and the structural refinement scheme of Jones et al. (1969), activity of the $Mg_9Si_4O_{16}(OH)_2$ end-member was estimated assuming ideal mixing on all the sites (aChu=0.1, Table 1). But since reaction topologies essentially depend on the absolute activity value of the phases (independent of the activity-composition relations), additional calculations were also made for aChu=0.3 and aClc=0.7 (Fig.4 b, d, f) in order to investigate the extent to which the phase stability limits are dependent on the activities. The activities of the phases that are absent in the studied rocks are considered unity (minimum stability). Similar petrological modeling in simplified systems, using activity-constrained end-members to discuss the effects of non-system components, is a useful tool to qualitatively discuss mineral evolution in many natural systems, particularly in fluid saturated metacarbonate rocks, where all necessary thermodynamic data and solid-solution models are not available (Connolly and Trommsdorff 1991; Castelli et al. 2007; Groppo et al. 2007; 2017; Dey et al. 2019).

Fig. 4g demonstrates the relative volume changes of the reactant and product phases along the texturally modeled reactions 1 and 2 respectively. The calculated topologies constrain the stability of the assemblage clinohumite + calcite + dolomite + forsterite ± spinel in the studied marbles at ~5-6 kbar pressures, at ~650-700°C in the presence of hydrous fluids. The results are similar to published studies constraining clinohumite formation in regionally metamorphosed marbles from other localities worldwide (Franz and Ackermand 1980; Rice 1980; Ríos et al. 2015).

This is the peer-reviewed, final accepted version for American Mineralogist, published by the Mineralogical Society of America.
The published version is subject to change. Cite as Authors (Year) Title. American Mineralogist, in press.
DOI: https://doi.org/10.2138/am-2021-7755. http://www.minsocam.org/

DISCUSSION

Mineral evolution in an open system

Petrographic observations and textural modeling indicates that clinohumite + spinel formed from a pre-existing assemblage most likely comprising calcite + dolomite + forsterite + chlorite. Whereas calcite + dolomite + forsterite was ubiquitously present in the whole rock, chlorite possibly occurred only in restricted domains. The clinohumite and spinel forming reactions (1 and 2) require the presence of free fluids, and Putnis (2002) suggested that due to the high molar volume of free fluids compared to the solid hydrous phases (e.g. chlorite, clinohumite), hydration reactions tend to have negative volume change (ΔV_{SOLID}), which in turn enhances the porosity of the rock, facilitating further fluid influx. The centimeter thick brown to brownish grey colored clinohumite and spinel bearing layers thus indicate the fluid flow channels. Compositionally, the host rock is devoid of any Ti-bearing accessory phase (like rutile, titanite, ilmenite, etc.). The major minerals of the host rock forsterite + dolomite are also devoid of Ti, F and OH (H_2O), all of which are present in clinohumite. Even chlorite, though a hydrous phase is not known to contain significant F or Ti (Rice 1980). So Ti and F was most likely transported by the H_2O-rich fluids from outside the system. Hence, the infiltration of free fluids transporting new components into the system indicates that the clinohumite and spinel forming reactions (1 and 2) occurred in an open system. Spinel formation is restricted only to the previously chlorite bearing domains (grey bands). Owing to the ubiquitous presence of forsterite + dolomite in the whole rock, clinohumite forms only where the infiltrated fluids affected this assemblage (brown layers).

Forsterite remains preserved elsewhere (the white to greyish white host rock) and is not replaced by any hydrous phase like serpentine, tremolite or brucite, which in turn indicates that fluid flow was not pervasive. The morphological features of the clinohumite ± spinel bands, like uniform thickness, fairly sharp boundaries, lateral continuity and mostly parallel sometimes anastomosing nature indicate that the fluid infiltration was highly channelized and restricted within the centimeter thick bands.

Formation of spinel and source of Al

Corundum solubility experiments indicate that the combined effects of pressure, temperature and the presence of dissolved alkalis, SiO_2 (albite) and halides (F and Cl) in aqueous fluids significantly increases Al solubility by the formation of Na/K-Al-Si-O clusters and/or polymers (Manning 2006; 2007; Tropper and Manning 2007; Newton and Manning 2008; Lucassen et al. 2010). In accordance with the experimental studies, the reported geological manifestations of fluid-mediated Al mobility are also in the form of quartz veins containing Al_2SiO_5 polymorphs ± biotite (in the wall rock) in regional metamorphic terrains (Kerrick 1988; Ague 1995; WhitneyDilek 2000; McLelland et al. 2002; Sepahi et al. 2004). Hence, the mineralogy of the studied rocks, particularly the absence of quartz, sillimanite and any Na/K-bearing phase with spinel does not support that Al was mobile in the present case.

If Al remained conserved, then, from Fig. 4g, in order to form ~12 vol% spinel in a layer, it had to contain ~40-45 vol% clinochlore/Mg-chlorite initially. Such chlorite rich layers are indeed common in dolomitic limestones and they represent clay layers of primary sedimentary origin (Bucher and Frey 2002). During regional metamorphism of the impure marbles, the clay layers form chlorite and then spinel during prograde metamorphism, whereas chlorite can form during

306 retrogression (Rice 1977; Bucher-Nurminen 1981; Sharp and Buseck 1988; Bucher and Frey
307 1994; 2002; Novak and Houzar 1996; Buick et al. 1997; Tropper et al. 2003; Castelli et al. 2007;
308 Groppo et al. 2007; Proyer et al. 2008; 2014; Rapa et al. 2017). Moreover, in the studied marbles,
309 spinel does not always occur with clinohumite, but only in some of the layers (grey bands). So,
310 while it is possible that the F- and Ti-bearing hydrous fluids might have carried minor Al form
311 outside, the predominant source of Al for spinel is more likely to be pre-existing
312 chlorite/clinochlore. Owing to the schistose habit of chlorite, the chlorite rich bands possibly
313 provided easier pathways for the fluids, and hence chlorite is no longer preserved.
314
315 **P–T–fluid regime of clinohumite formation**
316
317 During regional metamorphism, though forsterite marbles are usually diagnostic of granulite-
318 facies conditions (5-8 kbar, 700-800°C), forsterite can be produced at slightly lower temperatures
319 through interaction with an externally derived H_2O-rich fluid (Bucher and Frey 2002). However,
320 chlorite remains stable at all metamorphic grades below the granulite-facies (Bucher and Frey
321 2002). Hence, prior to fluid infiltration and the formation of clinohumite + spinel, the initial
322 assemblage calcite + dolomite + forsterite + chlorite was stabilized possibly during amphibolite-
323 facies metamorphism. So, the iT-P-X_{CO2} diagram was calculated at 600°C (Fig. 4a) and the iP-T-
324 X_{CO2} diagram was calculated at 5-6 kbar pressures in order to examine the domains of the
325 forsterite-in and spinel-in reactions (Fig. 4c). Rice (1980) has shown that that for X_F-clinohumite
326 <0.4, the clinohumite forming reaction (1) in the CMASV system is restricted to extremely low
327 X_{CO2} values (<0.1). With this knowledge in mind, the P/T-X topologies were calculated for H_2O-
328 rich fluids having $X_{CO2} < 0.03$; Also, based on the iT-P-X_{CO2} and the iP-T-X_{CO2} diagrams, the

329 mixed fluid-P-T diagram was constructed at fixed X_{CO2}=0.13 (Fig. 4e). The figures indicate that:

330 1. The reaction-1 [Dol+Fo→Cal+Chu] is the primary clinohumite forming reaction in the
331 CMASV system.
332 2. The assemblage clinohumite + calcite + dolomite + spinel is not only highly dependent on
333 pressure, with a decrease of the stability field as the pressure increases becoming extremely
334 restricted above ~6-7 kbar pressure, but is also restricted to very H_2O-rich fluid compositions
335 (X_{CO2}<0.02; Fig. 4a).
336 3. At ~5-6 kbar pressures, clinohumite + spinel is present above ~600°C temperature (Fig. 4c, e).

337 Additional calculations with reduced activity of clinochlore (aClc=0.7; green dashed lines
338 in Fig. 4b, d, f) show that there is no significant shift in the spinel forming reaction-2 in P-T-X
339 spaces. Calculations with increased activity of clinohumite (aChu=0.3; red dashed lines in Fig.
340 4b, d, f) demonstrate that:

341 1. There is a significant shift in reaction-1 to even more H_2O-rich fluid compositions
342 (X_{CO2}<0.01; Fig. 4b) and higher temperatures >700°C (Fig. 4d, f).
343 2. For aChu>0.1, reaction-2 [Dol+Clc→Cal+Chu+Spl] is no longer stable, and the reaction on
344 the opposite side of the invariant point [9] becomes the stable spinel forming reaction
345 [Dol+Clc→Cal+Fo+Spl] (Fig. 4b, d).
346 3. For aChu>0.3, the assemblage calcite + brucite becomes stable prior to calcite + clinohumite
347 (Fig. 4b, d, f). But the absence of brucite in the studied rocks indicates that absolute value of
348 activity of clinohumite was indeed <0.3, which is independent of the activity-composition
349 relationships that govern how the non-CMASH components are incorporated.
350 4. The low activity values of clinohumite also mean that the presence of F and Ti is the primary
351 cause for stabilizing clinohumite in the studied rocks.

5. The absence of brucite in the studied rocks brackets the stability of the assemblage clinohumite + calcite + dolomite + spinel to below 700°C (Fig. 4d, f).

In summary, the calculated topologies thus indicate that clinohumite grew in the studied forsterite marbles at ~5-6 kbar pressures and ~650-700°C in the presence of F-bearing hydrous fluids having X_{CO2}<0.03 (the field of clinohumite + spinel in Fig. 4). Forsterite remains stable in the host rocks unaffected by the infiltrating fluids. The fugacity of HF in equilibrium with the assemblage clinohumite-bearing assemblage with X_F<0.4 over the temperature range of 600-700°C is extremely low, ranging from 0.002 bars to 0.008 bars (Rice 1980). But such small amounts of HF in the fluid are not likely to have a measurable effect on the properties of the dominant CO_2-H_2O mixture. The stability of clinohumite was further facilitated by the presence of Ti in the fluids.

Ti mobility during regional metamorphism

The foregoing discussion clearly demonstrates that clinohumite formed in the rock due to infiltration of Ti and F bearing H_2O-rich fluids. The results are in accordance with experimental studies that solubility of Ti significantly increases in the presence of halides in aqueous fluids, especially F, by forming soluble complexes with the F- and Cl- ions (Ryzhenko et al. 2006; Antignano and Manning 2008; Purtov and Kotel'nikova 2010; Rapp et al. 2010; Hayden and Manning 2011; Tanis et al. 2016). Though Ti can be mobile in alkali-Si bearing hydrous fluids, like Al (Antignano and Manning 2008; Lucassen et al. 2010; Hayden and Manning 2011), but Ti content in the hydrous fluids is dominantly influenced the content of halides, with solubilities greater in fluoride than in chloride solutions, and in acid than in neutral or alkaline solutions

(Purtov and Kotel'nikova 2010). The Ti-bearing fluids also affected the spinel-magnetite compositions as magnetite occurring at the core of the spinel grains also contain 0.6-0.9 wt% TiO_2. The presence of the clinohumite ± spinel bands over several kilometers across multiple outcrops indicates that Ti and F were mobile at least at kilometer scale.

The source of the Ti-F-H_2O-fluids is however not absolutely clear. As already mentioned, the studied area contains abundant intrusions of a suite of mafic rocks (Fig. 1). These mafic rocks dominantly comprise recrystallized amphibole + plagioclase, but relicts of the primary magmatic minerals (F-apatite, ilmenite, olivine) are still present. So the most likely scenario seems to be that, during infiltration driven regional metamorphism, the aqueous fluids hydrated and altered the mafic rocks, thereby becoming enriched in F and dissolving Ti (ilmenite). This Ti-F rich fluid then led to alteration of the nearby marbles, forming clinohumite.

IMPLICATIONS

Ti is essentially considered immobile in common metamorphic systems due to its retention in rutile, ilmenite, and titanite at the source and low TiO_2 solubility in common metamorphic fluids (Audétat and Keppler 2005; Tropper and Manning 2005). As a consequence, the constant-Ti frame of reference is widely used in most mass-flux calculations in fluid transport and to evaluate open-system behavior during metasomatism. Also, the low mobility of Ti and other HFSEs is one of the suggested sources of the HFSE depletion observed in all arc magmas. However, natural examples and experimental studies have shown that Ti can be significantly mobile in F-bearing aqueous fluids. This compositional dependence of Ti solubility not only questions a fundamental premise of most mass-flux calculations, but also has implications for HFSE mobility during metamorphic processes, and consequently in the understanding of trace element recycling during

crustal processes. Therefore, the assumption of Ti immobility, and use of Ti as a chemical frame of reference, is not universally valid and should be used with caution.

Acknowledgements

I acknowledge the financial support from the University Grant Commission (UGC), India, under the "Dr. D. S. Kothari" post-doctoral fellowship scheme, and thank my mentor Pulak Sengupta for his time and comments during the preparation of this manuscript. I thank my colleagues Prithwiraj Maity, Sustava Bhattacharya, Mohai Menul Hassan and Arimita Chakrabarty for their participation and contributions during field work. I sincerely appreciate the encouraging positive feedback and insightful comments from my reviewers Chiara Groppo and Cyril Durand. I also thank Thomas Mueller for his effective editorial handling.

REFERENCES CITED

Acharyya, S.K. (2003) The Nature of Mesoproterozoic Central Indian Tectonic Zone with Exhumed and Reworked Older Granulites. Gondwana Research, 6, 197–214.

Ague, J.J. (1995) Deep crustal growth of quartz, kyanite and garnet into large-aperture, fluid-filled fractures, north-eastern Connecticut, USA. Journal of Metamorphic Geology, 13, 299–314.

Ague, J.J. (2003) Fluid infiltration and transport of major, minor, and trace elements during regional metamorphism of carbonate rocks, Wepawaug Schist, Connecticut, USA. American Journal of Science, 303, 753–816.

Antignano, A., and Manning, C.E. (2008) Rutile solubility in H2O, H2O–SiO2, and H2O–NaAlSi3O8 fluids at 0.7–2.0 GPa and 700–1000 °C: Implications for mobility of nominally insoluble elements. Chemical geology, 255, 283–293.

Audétat, A., and Keppler, H. (2005) Solubility of rutile in subduction zone fluids, as determined by experiments in the hydrothermal diamond anvil cell. Earth and Planetary Science Letters,

232, 393–402.

Bhattacharyya, C. (1974) Clinohumite marble from Vemali, Srikakulam District, Andhra Pradesh, India. Mineralogical Magazine, 39, 727–729.

Bhowmik, S.K. (2019) The current status of orogenesis in the Central Indian Tectonic Zone: A view from its Southern Margin. (M. Santosh, Ed.)Geological Journal, 64, 17.

Bucher, K., and Frey, M. (1994) Metamorphism of Marls. In K. Bucher and M. Frey, Eds., Petrogenesis of Metamorphic Rocks: Complete Revision of Winkler's Textbook pp. 233–250. Springer Berlin Heidelberg, Berlin, Heidelberg.

Bucher, K., and Frey, M. (2002) Metamorphism of Dolomites and Limestones. In K. Bucher and M. Frey, Eds., Petrogenesis of Metamorphic Rocks pp. 197–216. Springer Berlin Heidelberg, Berlin, Heidelberg.

Bucher-Nurminen, K. (1981) Petrology of chlorite-spinel marbles from NW Spitsbergen (Svalbard). Lithos, 14, 203–213.

Buick, I.S., Cartwright, I., and Williams, I. (1997) High-temperature Retrogression of Granulite-facies Marbles form the Reynolds Range Group, Central Australia: Phase Equilibria, Isotopic Resetting and Fluid Fluxes. Journal of Petrology, 38, 877–910.

Castelli, D., RoLFo, F., Groppo, C., and Compagnoni, R. (2007) Impure marbles from the UHP Brossasco-Isasca Unit (Dora-Maira Massif, western Alps): evidence for Alpine equilibration in the diamond stability field and evaluation of the X(CO 2) fluid evolution. Journal of Metamorphic Geology, 25, 587–603.

Chattopadhyay, N., Sengupta, P., and Mukhopadhyay, D. (2009) Reaction textures in a suite of clinohumite - forsterite bearing marbles from parts of the Grenvillian South Delhi Fold Belt, India: Evidence of Ti mobility during regional metamorphism p. 3221. Presented at the European Geosciences Union General Assembly, Vienna, Austria.

Chowdhury, P., Talukdar, M., Sengupta, P., Sanyal, S., and Mukhopadhyay, D. (2013) Controls of P-T path and element mobility on the formation of corundum pseudomorphs in Paleoproterozoic high-pressure anorthosite from Sittampundi, Tamil Nadu, India. American Mineralogist, 98, 1725–1737.

Connolly, J. (2005) Computation of phase equilibria by linear programming: a tool for geodynamic modeling and its application to subduction zone decarbonation. Earth and Planetary Science Letters, 236, 524–541.

Connolly, J. (2009) The geodynamic equation of state: What and how. Geochemistry Geophysics Geosystems, 10, 1–19.

Connolly, J., and Trommsdorff, V. (1991) Petrogenetic grids for metacarbonate rocks: pressure-temperature phase-diagram projection for mixed-volatile systems. Contributions to Mineralogy and Petrology, 108, 93–105.

463 Deshmukh, T., Prabhakar, N., Bhattacharya, A., and Madhavan, K. (2017) Late Paleoproterozoic
464 clockwise P-T history in the Mahakoshal Belt, Central Indian Tectonic Zone: Implications
465 for Columbia supercontinent assembly. Precambrian Research, 298, 56–78.

466 Dey, A., Choudhury, S.R., Mukherjee, S., Sanyal, S., and Sengupta, P. (2019) Origin of
467 vesuvianite-garnet veins in calc-silicate rocks from part of the Chotanagpur Granite Gneiss
468 Complex, East Indian Shield: The quantitative P-T-XCO2 topology in parts of the system
469 CaO-MgO-Al2O3-SiO2-H2O-CO2 (+Fe2O3, F). American Mineralogist, 104, 744–760.

470 Duffy, C.J., and Greenwood, H.J. (1979) Phase equilibria in the system MgO-MgF2-SiO2-H2O.
471 American Mineralogist, 64, 1156–1174.

472 Dymek, R.F., Boak, J.L., and Brothers, S.C. (1988) Titanian chondrodite- and titanian
473 clinohumite-bearing metadunite from the 3800 Ma Isua supracrustal belt, West Greenland:
474 Chemistry, petrology and origin**.** American Mineralogist, 73, 547–558.

475 Ehlers, K., and Hoinkes, G. (1987) Titanian chondrodite and clinohumite in marbles from the
476 Ötztal crystalline basement. Mineralogy and Petrology, 36, 13–25.

477 Evans, B.W., and Trommsdorff, V. (1983) Fluorine hydroxyl titanian clinohumite in Alpine
478 recrystallized garnet peridotite: compositional controls and petrologic significance. American
479 Journal of Science, 283-A, 355–369.

480 Fernandes, M.L.S., and Chaves, A.O. (2014) Chemical composition and genesis of the
481 clinohumites from marbles of Itaoca-Gironda, Espírito Santo State, Brazil. Comunicações
482 Geológicas, 101, 81–84.

483 Fisher, G.W. (1989) Matrix analysis of metamorphic mineral assemblages and reactions.
484 Contributions to Mineralogy and Petrology, 102, 69–77.

485 Franz, G., and Ackermand, D. (1980) Phase relations and metamorphic history of a clinohumite-
486 chlorite-serpentine-marble from the Western Tauern Area (Austria). Contributions to
487 Mineralogy and Petrology, 75, 97–110.

488 Gaspar, J.C. (1992) Titanian clinohumite in the carbonatites of the Jacupiranga Complex, Brazil:
489 mineral chemistry and comparison with titanian clinohumite from other environments.
490 American Mineralogist, 77, 168–178.

491 Gieré, R. (1987) Titanian clinohumite and geikielite in marbles from the Bergell contact aureole.
492 Contributions to Mineralogy and Petrology, 96, 496–502.

493 González-Jiménez, J.M., Plissart, G., Garrido, L.N., Pardón-Navarta, J.A., Aiglsperger, T.,
494 Romero, R., Marchesi, C., Moreno-Abril, A.J., Reich, M., Barra, F., and others (2017) Ti-
495 clinohumite and Ti-chondrodite in antigorite serpentinites from Central Chile: evidence for
496 deep and cold subduction. European Journal of Mineralogy, 29, 959–970.

497 Grew, E.S., Locock, A.J., Mills, S.J., Galuskina, I.O., Galuskin, E.V., and Hålenius, U. (2013)
498 Nomenclature of the garnet supergroup. American Mineralogist, 98, 785–811.

499 Groppo, C., and Compagnoni, R. (2007) Metamorphic veins from the serpentinites of the
500 Piemonte Zone, western Alps, Italy: a review. Periodico di Mineralogia, 76, 1–28.

501 Groppo, C., Castelli, D., and RoLFo, F. (2007) HT, pre-Alpine relics in a spinel-bearing dolomite
502 marble from the UHP Brossasco-Isasca Unit (Dora-Maira Massif, Western Alps, Italy).
503 Periodico di Mineralogia, 76, 155–168.

504 Groppo, C., Rolfo, F., Castelli, D., and Mosca, P. (2017) Metamorphic CO2 Production in
505 Collisional Orogens: Petrological Constraints from Phase Diagram Modeling of Himalayan,
506 Scapolite-bearing, Calc-silicate Rocks in the NKC(F)MAS(T)-HC system. Journal of
507 Petrology, 58, 53–83.

508 Grützner, T., Klemme, S., Rohrbach, A., Gervasoni, F., and Berndt, J. (2017) The role of F-
509 clinohumite in volatile recycling processes in subduction zones. Geology, 45, 443–446.

510 Hayden, L.A., and Manning, C.E. (2011) Rutile solubility in supercritical NaAlSi3O8–H2O
511 fluids. Chemical geology, 284, 74–81.

512 Holland, Tim, and Powell, R. (2015) AX: a program to calculate activities of mineral
513 endmembers from chemical analyses. University of Cambridge.

514 Holland, TJB, and Powell, R. (1998) An internally consistent thermodynamic data set for phases
515 of petrological interest. Journal of Metamorphic Geology, 16, 309–343.

516 Jiang, S.-Y., Wang, R.-C., Xu, X.-S., and Zhao, K.-D. (2005) Mobility of high field strength
517 elements (HFSE) in magmatic-, metamorphic-, and submarine-hydrothermal systems.
518 Physics and Chemistry of the Earth, Parts A/B/C, 30, 1020–1029.

519 Jones, N.W., Ribbe, P.H., and American, G.G. (1969) Crystal chemistry of humite minerals.
520 American Mineralogist, 54, 391–411.

521 Karmakar, S., Mukherjee, S., Sanyal, S., and Sengupta, P. (2017) Origin of peraluminous
522 minerals (corundum, spinel, and sapphirine) in a highly calcic anorthosite from the
523 Sittampundi Layered Complex, Tamil Nadu, India. Contributions to Mineralogy and
524 Petrology, 172, 1–23.

525 Kerrick, D.M. (1988) Al2SiO5-bearing segregations in the Lepontine Alps, Switzerland:
526 Aluminum mobility in metapelites. Geology, 16, 636.

527 Lang, H.M., Wachter, A.J., Peterson, V.L., and Ryan, J.G. (2004) Coexisting
528 clinopyroxene/spinel and amphibole/spinel symplectites in metatroctolites from the Buck
529 Creek ultramafic body, North Carolina Blue Ridge. American Mineralogist, 89, 20–30.

530 Lucassen, F., Franz, G., Rhede, D., and Wirth, R. (2010) Ti-Al zoning of experimentally grown
531 titanite in the system CaO-Al2O3-TiO2-SiO2-NaCl-H2O-(F): Evidence for small-scale fluid
532 heterogeneity. American Mineralogist, 95, 1365–1378.

533 Manning, C.E. (2006) Mobilizing aluminum in crustal and mantle fluids. Journal of Geochemical

534 Exploration, 89, 251–253.

535 Manning, C.E. (2007) Solubility of corundum + kyanite in H 2O at 700°C and 10 kbar:
536 evidence for Al-Si complexing at high pressure and temperature. Geofluids, 7, 258–269.

537 McLelland, J., Morrison, J., Selleck, B., Cunningham, B., Olson, C., and Schmidt, K. (2002)
538 Hydrothermal alteration of late- to post-tectonic Lyon Mountain Granitic Gneiss, Adirondack
539 Mountains, New York: Origin of quartz-sillimanite segregations, quartz-albite lithologies,
540 and associated Kiruna-type low-Ti Fe-oxide deposits. Journal of Metamorphic Geology, 20,
541 175–190.

542 Muthuswami, T.N. (1958) Clinohumite sausar series, Bhandara district, India. Proceedings of the
543 Indian Academy of Sciences - Section A, 48, 9–28.

544 Newton, R.C., and Manning, C.E. (2008) Solubility of corundum in the system Al2O3–SiO2–
545 H2O–NaCl at 800 °C and 10 kbar. Chemical geology, 249, 250–261.

546 Nishio, I., Morishita, T., Szilas, K., Pearson, G., Tani, K.-I., Tamura, A., Harigane, Y., and
547 Guotana, J. (2019) Titanian Clinohumite-Bearing Peridotite from the Ulamertoq Ultramafic
548 Body in the 3.0 Ga Akia Terrane of Southern West Greenland. Geosciences, 9, 153–20.

549 Novak, M., and Houzar, S. (1996) The HT/LP metamorphism of dolomite marbles in the eastern
550 part of the Moldanubicum; A manifestation of heat flow related to the Trebic Durbachite
551 Massif. Journal of Czech Geological Society, 41, 139–146.

552 Okay, A.I. (1994) Sapphirine and Ti-clinohumite in ultra-high-pressure garnet-pyroxenite and
553 eclogite from Dabie Shan, China. Contributions to Mineralogy and Petrology, 116, 145–155.

554 Pawley, A. (2000) Stability of clinohumite in the system MgO-SiO2-H2O. Contributions to
555 Mineralogy and Petrology, 138, 284–291.

556 Piazolo, S., and Markl, G. (1999) Humite-and scapolite-bearing assemblages in marbles and
557 calcsilicates of Dronning Maud Land, Antarctica: new data for Gondwana reconstructions.
558 Journal of Metamorphic Geology, 17, 91–107.

559 Pouchou, J.L., and Pichoir, F. (1984) A new model for quantitative X-ray microanalysis. I. -
560 application to the analysis of homogeneous samples. La Recherche Aérospatiale, 3, 167–192.

561 Pradeepkumar, A.P., and Krishnanath, R. (2000) A Pan-African “humite epoch”in East
562 Gondwana: implications for Neoproterozoic Gondwana geometry. Journal of Geodynamics,
563 29, 43–62.

564 Proyer, A., Baziotis, I., Mposkos, E., and Rhede, D. (2014) Ti- and Zr-minerals in calcite-
565 dolomite marbles from the ultrahigh-pressure Kimi Complex, Rhodope mountains, Greece:
566 Implications for the P-T evolution based on reaction textures, petrogenetic grids, and
567 geothermobarometry. American Mineralogist, 99, 1429–1448.

568 Proyer, A., Mposkos, E., Baziotis, I., and Hoinkes, G. (2008) Tracing high-pressure

metamorphism in marbles: Phase relations in high-grade aluminous calcite–dolomite marbles from the Greek Rhodope massif in the system CaO–MgO–Al2O3–SiO2–CO2 and indications of prior aragonite. Lithos, 104, 119–130.

Purtov, V.K., and Kotel'nikova, A.L. (2010) Solubility of Titanium in Chloride and Fluoride Hydrothermal Solutions. International Geology Review, 35, 279–287.

Putnis, A. (2002) Mineral replacement reactions: from macroscopic observations to microscopic mechanisms. Mineralogical Magazine, 66, 689–708.

Rahn, M.K., and Bucher, K. (1998) *Titanian Clinohumite Formation in the Zermatt-Saas Ophiolites, Central Alps*. Mineralogy and Petrology, 64, 1–13.

Rapa, G., Groppo, C., Rolfo, F., Petrelli, M., Pietro Mosca, and Perugini, D. (2017) Titanite-bearing calc-silicate rocks constrain timing, duration and magnitude of metamorphic CO2 degassing in the Himalayan belt. Lithos, 292-293, 364–378.

Rapp, J.F., Klemme, S., Butler, I.B., and Harley, S.L. (2010) Extremely high solubility of rutile in chloride and fluoride-bearing metamorphic fluids: An experimental investigation. Geology, 38, 323–326.

Rice, J.M. (1977) Contact metamorphism of impure dolomitic limestone in the Boulder Aureole, Montana. Contributions to Mineralogy and Petrology, 59, 237–259.

Rice, J.M. (1980) Phase equilibria involving humite minerals in impure dolomitic limestones. Part I. Calculated stability of clinohumite. Contributions to Mineralogy and Petrology, 71, 219–235.

Ríos, C.A., Castellanos, Ó.M., and Chacón, C.A. (2015) Ti-clinohumite in the Ciénaga skarn-type mineralogy, Sierra Nevada de Santa Marta Massif (Colombia): Occurrence and petrologic significance. Earth Sciences Research Journal, 19, 15–30.

Roy, A., and Prasad, M.H. (2003) Tectonothermal events in Central Indian Tectonic Zone (CITZ) and its implications in Rodinian crustal assembly. Journal of Asian Earth Sciences, 22, 115–129.

Ryzhenko, B.N., Kovalenko, N.I., and Prisyagina, N.I. (2006) Titanium complexation in hydrothermal systems. Geochemistry International, 44, 879–895.

Sarkar, A., Boda, M.S., Kundu, H.K., Mamgain, V.V., Ravishankar (1998) Geochronology and geochemistry of Mesoproterozoic intrusive plutonites from the eastern segment of the Mahakoshal greenstone belt, Central India Vol. Bhubaneshwar, India, pp. 82–85. Presented at the IGCP- Seminar on Precambrian Crust in Eastern and Central India, Bhubaneshwar, India.

Satish-Kumar, M., and Niimi, N. (1998) Fluorine-rich clinohumite from Ambasamudram marbles, southern India: mineralogical and preliminary FTIR spectroscopic characterization. Mineralogical Magazine, 62, 509–519.

Sánchez-Vizcaíno, V.L., Trommsdorff, V., Gómez-Pugnaire, M.T., Garrido, C.J., Müntener, O., and Connolly, J. (2005) Petrology of titanian clinohumite and olivine at the high-pressure breakdown of antigorite serpentinite to chlorite harzburgite (Almirez Massif, S. Spain). Contributions to Mineralogy and Petrology, 149, 626–646.

Scambelluri, M., and Rampone, E. (1999) Mg-metasomatism of oceanic gabbros and its control on Ti-clinohumite formation during eclogitization. Contributions to Mineralogy and Petrology, 135, 1–17.

Scambelluri, M., Strating, E.H.H., Piccardo, G.B., Vissers, R.L.M., and Rampone, E. (1991) Alpine olivine- and titanian clinohumite-bearing assemblages in the Erro-Tobbio peridotite (Voltri Massif, NW Italy). Journal of Metamorphic Geology, 9, 79–91.

Sengupta, P., and Dasgupta, S. (2009) Modelling of Metamorphic Textures with C-Space: Evidence of Pan-African High-grade Reworking in the Eastern Ghats Belt, India. In A.K. Gupta and S. Dasgupta, Eds., Physics and Chemistry of the Earth's Interior pp. 29–39. Springer New York, New York, NY.

Sepahi, A.A., Whitney, D.L., and Baharifar, A.A. (2004) Petrogenesis of andalusite-kyanite-sillimanite veins and host rocks, Sanandaj-Sirjan metamorphic belt, Hamadan, Iran. Journal of Metamorphic Geology, 22, 119–134.

Sharp, T.G., and Buseck, P. (1988) Prograde versus retrograde chlorite amphibole intergrowths in a calc-silicate rock. American Mineralogist, 73, 1292–1301.

Shen, T., Hermann, J., Zhang, L., Lü, Z., Padrón-Navarta, J.A., Xia, B., and Bader, T. (2015) UHP Metamorphism Documented in Ti-chondrodite- and Ti-clinohumite-bearing Serpentinized Ultramafic Rocks from Chinese Southwestern Tianshan. Journal of Petrology, 56, 1425–1458.

Stalder, R., and Ulmer, P. (2001) Phase relations of a serpentine composition between 5 and 14 GPa: significance of clinohumite and phase E as water carriers into the transition zone. Contributions to Mineralogy and Petrology, 140, 670–679.

Tanis, E.A., Simon, A., Zhang, Y., Chow, P., Xiao, Y., Hanchar, J.M., Tschauner, O., and Shen, G. (2016) Rutile solubility in NaF-NaC-KCl-bearing aqueous fluids at 0.5-2.79 GPa and 250-650 °C. Geochimica et Cosmochimica Acta, 177, 170–181.

Torres-Roldan, R.L., Garcia-Casco, A., and Garcia-Sanchez, P.A. (2000) CSpace: An integrated workplace for the graphical and algebraic analysis of phase assemblages on 32-bit Wintel platforms. Computers & Geosciences, 26, 779–793.

Trommsdorff, V., and Evans, B.W. (1980) Titanian hydroxyl-clinohumite: Formation and breakdown in antigorite rocks (Malenco, Italy). Contributions to Mineralogy and Petrology, 72, 229–242.

Tropper, P., and Manning, C.E. (2007) The solubility of corundum in H2O at high pressure and temperature and its implications for Al mobility in the deep crust and upper mantle.

Chemical geology, 240, 54–60.

Tropper, P., and Manning, C.E. (2005) Very low solubility of rutile in H2O at high pressure and temperature, and its implications for Ti mobility in subduction zones. American Mineralogist, 90, 502–505.

Tropper, P., Harlov, D., Krenn, E., Finger, F., Rhede, D., and Bernhard, F. (2007) Zr-bearing minerals as indicators for the polymetamorphic evolution of the eastern, lower Austroalpine nappes (Stubenberg Granite contact aureole, Styria, Eastern Alps, Austria). Lithos, 95, 72–86.

Tropper, P., Tessadri, R., and Konzett, J. (2003) Spinel-bearing carbonates as petrogenetic recorders of the Variscan pT evolution of the Austroalpine basement of the Otztal Complex (Tyrol, Austria). Journal of Czech Geological Society, 48, 129–130.

Whitney, D.L., and Evans, B.W. (2010) Abbreviations for names of rock-forming minerals. American Mineralogist, 95, 185–187.

Whitney, Dilek (2000) Andalusite–sillimanite–quartz veins as indicators of low-pressure–high-temperature deformation during late-stage unroofing of a metamorphic core complex, Turkey. Journal of Metamorphic Geology, 18, 59–66.

Wunder, B. (1998) Equilibrium experiments in the system MgO–SiO2–H2O (MSH): stability fields of clinohumite-OH [Mg9Si4O16(OH)2], chondrodite-OH [Mg5Si2O8(OH)2] and phase A (Mg7Si2O8(OH)6). Contributions to Mineralogy and Petrology, 132, 111–120.

Young, E.D., and Morrison, J. (1992) Relations among net-transfer reaction progress, 18O−13C depletion, and fluid infiltration in a clinohumite-bearing marble. Contributions to Mineralogy and Petrology, 111, 391–408.

FIGURE CAPTIONS

FIGURE 1. (a) Generalized geological map of part of the Central Indian Tectonic Zone (CITZ) after Roy and Prasad (2003) showing the studied area. **(b)** Map of the studied area showing the the major lithological distributions and sample locations of the studied banded marbles.

673 **FIGURE 2. (a)** Field photograph and **(b-c)** hand-specimen photographs showing the off-white to
674 greyish white colored saccharoidal marbles with brown colored clinohumite and grey colored
675 spinel-rich layers. **(d-e)** Back-scattered electron (BSE) microscopic images of the unaltered host
676 marbles showing a granoblastic texture defined by polygonal grains of dolomite and calcite (in
677 subequal proportions) and subordinate amount of forsterite. **(f)** Photomicrograph of brown band
678 (as in b) showing recrystallized polygonal clinohumite grains, with rounded forsterite relicts, and
679 minor calcite. **(g)** Photomicrograph of grey band (as in a or c) showing recrystallized spinel and
680 clinohumite grains. **(h, i)** Photomicrograph and BSE image showing recrystallized spinel grains
681 with magnetite at the core.
682
683 **FIGURE 3. (a)** Plot of OH + F vs. Ti (a.p.f.u. x 10^4) after Jones et al. (1969) showing the
684 efficiency of the exchange vector $TiO_2Mg_{-1}(F, OH)_{-2}$ in clinohumite. The data fall along the
685 straight line whose equation matches well with the theoretical equation (OH +F) = -2Ti + $2/9M_{Ti}$.
686 **(b)** Plot of TiO_2 vs. MgO/(MgO+MnO+FeO) after Rios et al. (2015) showing that the
687 composition of clinohumite of the studied marbles are similar to those from other marbles. **(c)**
688 Chemographic relations of the phases in the CaO-(MgO+FeO)-Al_2O_3-SiO_2 volume tetrahedron.
689 CO_2 and H_2O are considered excess. All the phases lie on the bounding surfaces of the
690 tetrahedron.
691
692 **FIGURE 4.** Phase topology in the fluid saturated CMASV (CaO-MgO-Al_2O_3-SiO_2-H_2O-CO_2)
693 system calculated in **(a-b)** isothermal Pressure vs. X_{CO2} space at 600°C; **(c-d)** isobaric
694 Temperature vs. X_{CO2} space at 5 kbar (similar topology at both pressures); and **(e-f)** mixed
695 volatile Pressure vs. Temperature space at fixed X_{CO2}=0.13. **(g)** Change in the relative modal

696 abundance of the different phases along the texturally modeled reactions 1 and 2. * indicates
697 phases whose activities were reduced based on their measured compositions: **(a, c, e)** aSpl=0.83,
698 aFo=0.94, aChu=0.1 and pure Clc; **(b, d, f)** red dashed lines for aChu=0.3 and green dashed lines
699 for aClc=0.7. The calculated topologies constrain the stability of the assemblage clinohumite +
700 calcite + dolomite + spinel (± forsterite) in the studied marbles at ~5-6 kbar pressures, at ~650-
701 700°C in the presence of hydrous fluids with X_{CO2}<0.03.
702

Fig. 1

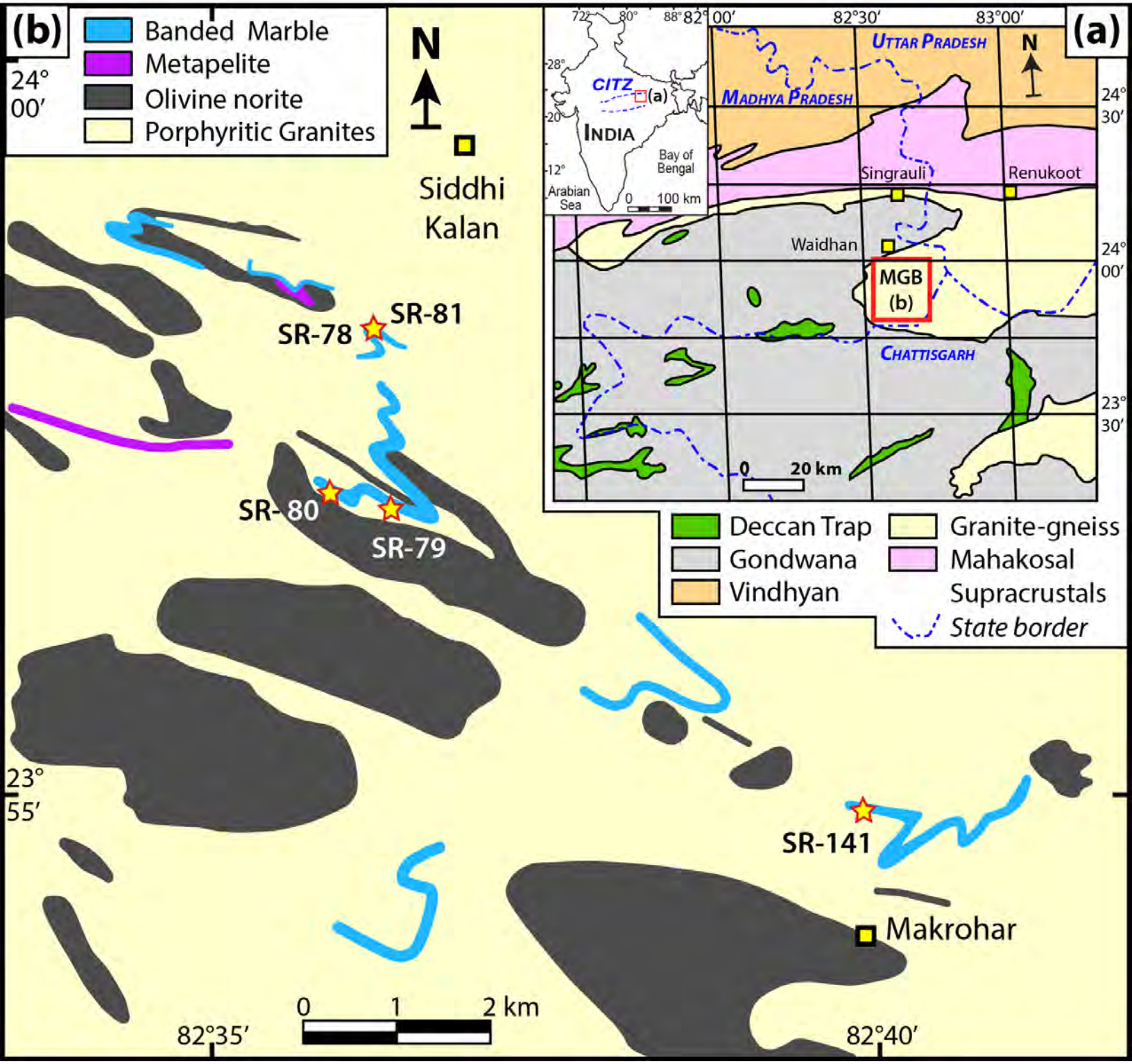
(b)
Banded Marble
Metapelite
Olivine norite
Porphyritic Granites
24° 00′
N
Siddhi Kalan
SR-78
SR-81
SR-80
SR-79
SR-141
Makrohar
23° 55′
82°35′
82°40′
0 1 2 km
(a)
72°
80°
88°
82°
28°
20°
12°
CITZ
(a)
INDIA
Bay of Bengal
Arabian Sea
0 100 km
82°00′
82°30′
83°00′
UTTAR PRADESH
MADHYA PRADESH
N
24° 30′
24° 00′
23° 30′
Singrauli
Renukoot
Waidhan
MGB (b)
CHATTISGARH
0 20 km
Deccan Trap
Gondwana
Vindhyan
Granite-gneiss
Mahakosal
Supracrustals
State border

Fig. 2

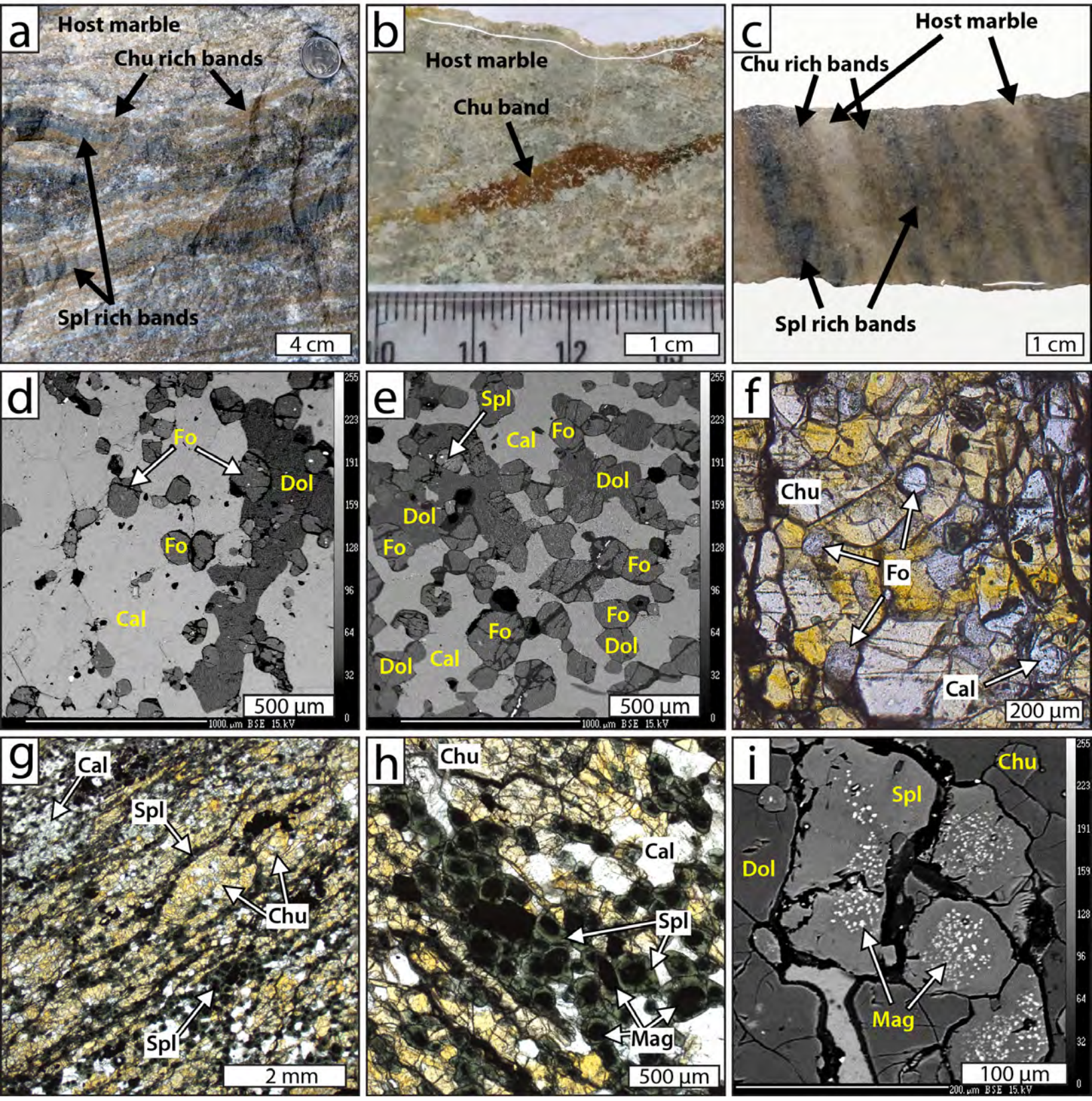
a
Host marble
Chu rich bands
Spl rich bands
4 cm
b
Host marble
Chu band
1 cm
c
Host marble
Chu rich bands
Spl rich bands
1 cm
d
Fo
Dol
Fo
Cal
500 µm
1000. µm BSE 15.kV
e
Spl
Cal
Fo
Dol
Dol
Fo
Fo
Fo
Dol
Dol
Cal
500 µm
1000. µm BSE 15.kV
f
Chu
Fo
Cal
200 µm
g
Cal
Spl
Chu
Spl
2 mm
h
Chu
Cal
Spl
Mag
500 µm
i
Chu
Spl
Dol
Mag
100 µm
200. µm BSE 15.kV

Fig. 3

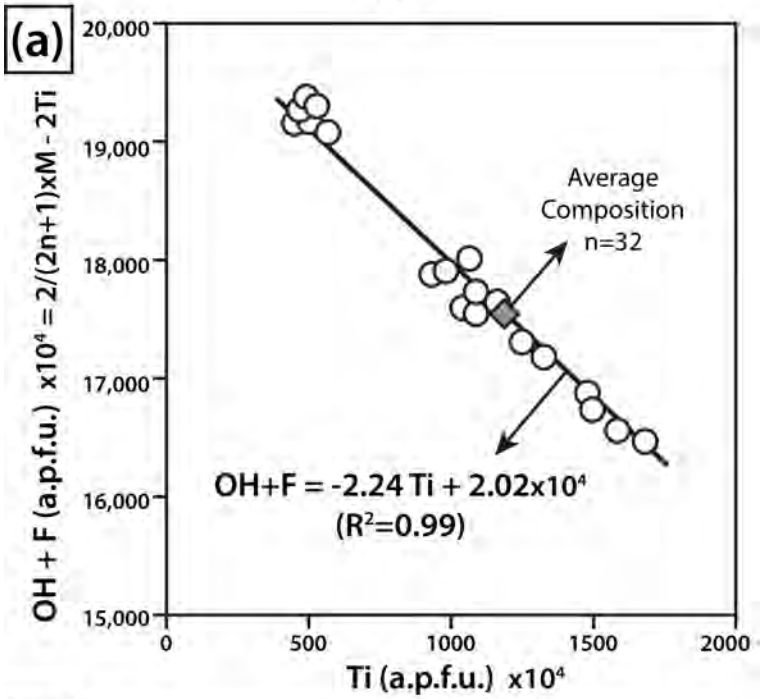
(a)
20,000
19,000
18,000
17,000
16,000
15,000
OH + F (a.p.f.u.) x10⁴ = 2/(2n+1)xM - 2Ti
Average
Composition
n=32
OH+F = -2.24 Ti + 2.02x10⁴
(R²=0.99)
0
500
1000
1500
2000
Ti (a.p.f.u.) x10⁴

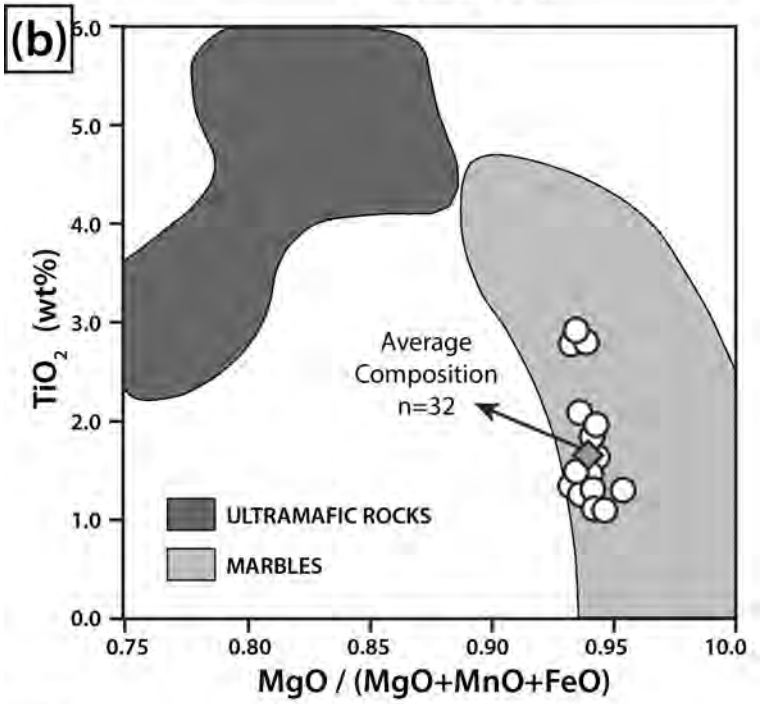
(b)
6.0
5.0
4.0
3.0
2.0
1.0
0.0
TiO₂ (wt%)
Average
Composition
n=32
ULTRAMAFIC ROCKS
MARBLES
0.75
0.80
0.85
0.90
0.95
10.0
MgO / (MgO+MnO+FeO)

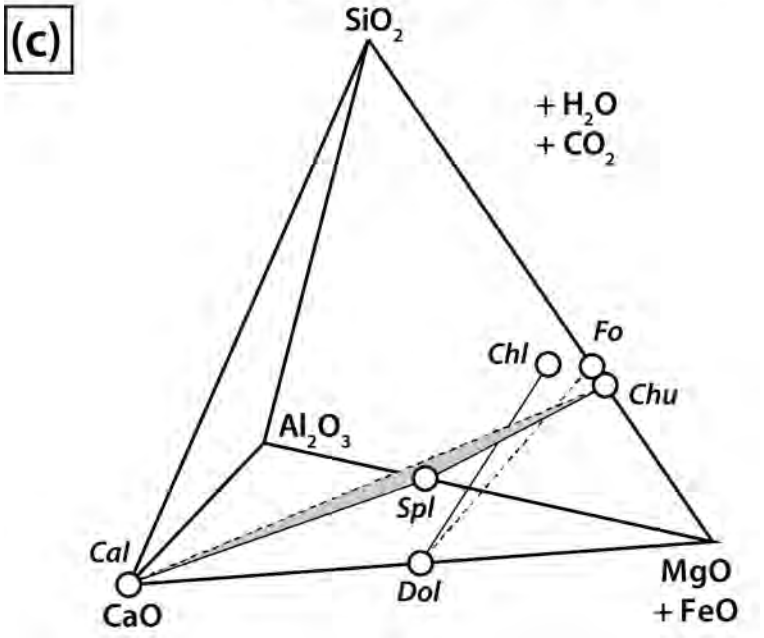
(c)
SiO₂
+ H₂O
+ CO₂
Fo
Chl
Chu
Al₂O₃
Spl
Cal
Dol
MgO
+ FeO
CaO

Fig. 4

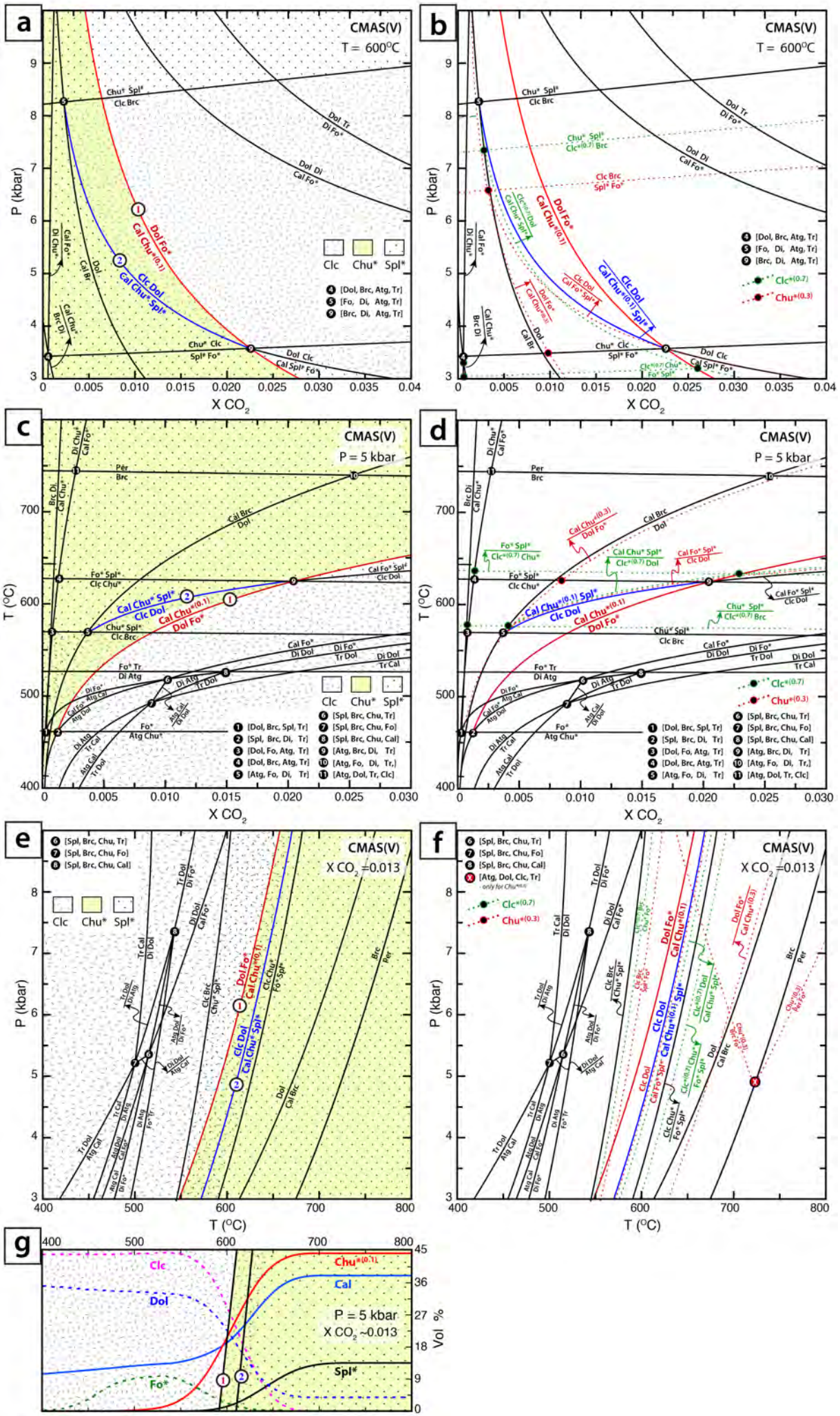
a
CMAS(V)
T = 600°C
P (kbar)
X CO2
Clc
Chu*
Spl*
b
CMAS(V)
T = 600°C
P (kbar)
X CO2
c
CMAS(V)
P = 5 kbar
T (°C)
X CO2
d
CMAS(V)
P = 5 kbar
T (°C)
X CO2
e
CMAS(V)
X CO2 =0.013
P (kbar)
T (°C)
f
CMAS(V)
X CO2 =0.013
P (kbar)
T (°C)
g
P = 5 kbar
X CO2 ~0.013
Vol %
Clc
Dol
Cal
Chu*(0.1)
Fo*
Spl*

Table 1: Representative microprobe analyses and calculated cations of forsterite, spinel, magnetite and clinohumite (n=

Sample	SR141	SR79	SR78	*Average*		SR141	SR79	SR78	*Average*		SR79
Mineral	Fo	Fo	Fo	*Fo*		Spl	Spl	Spl	*Spl*		Mag
Point	50	55	87^{TM}	*n=32*	*±2σ*	110	51	101^{TM}	*n=15*	*±2σ*	35
SiO_2	42.12	41.59	41.61	*41.69*	*2.40*	0.09	0.03	0.09	*0.04*	*0.07*	0.02
TiO_2	0.04	0.02	0.02	*0.04*	*0.27*	0.10	0.03	0.05	*0.05*	*0.04*	0.92
Al_2O_3	0.03	0.01	0.02	*-0.01*	*0.04*	62.75	65.33	66.47	*64.70*	*2.84*	0.37
Cr_2O_3	0.01	0.02	0.01	*0.00*	*0.03*	0.08	0.08	0.07	*0.07*	*0.04*	0.08
Fe_2O_3*	--	--	--	--	--	7.99	4.60	3.67	*5.36*	*3.35*	66.74
FeO*	3.65	4.16	4.14	*3.74*	*0.58*	6.17	4.91	5.99	*5.31*	*1.30*	27.86
MnO	0.33	0.46	0.31	*0.31*	*0.24*	0.43	0.21	0.12	*0.17*	*0.18*	0.24
MgO	52.87	53.41	53.44	*53.19*	*1.43*	23.26	24.19	23.94	*23.91*	*0.92*	2.13
ZnO	--	--	--	--	--	b.d.l.	b.d.l.	0.08	*0.02*	*0.06*	b.d.l.
CaO	0.05	0.02	0.05	*0.05*	*0.06*	--	--	--	--	--	--
TOTAL	99.10	99.74	99.60	*99.03*	*3.07*	100.90	99.48	100.46	*99.69*	*1.06*	98.43
Oxygen basis	4	4	4	--	--	4	4	4	--	--	4
Si	1.01	1.00	1.00	*1.00*	*0.03*	0.00	0.00	0.00	*0.00*	*0.00*	0.00
Ti	0.00	0.00	0.00	*0.00*	*0.00*	0.00	0.00	0.00	*0.00*	*0.00*	0.03
Al	0.00	0.00	0.00	*0.00*	*0.00*	1.84	1.91	1.92	*1.89*	*0.06*	0.02
Cr	0.00	0.00	0.00	*0.00*	*0.00*	0.00	0.00	0.00	*0.00*	*0.00*	0.00
Fe^{+3}*	--	--	--	--	--	0.15	0.09	0.07	*0.10*	*0.06*	1.93
Fe^{+2}*	0.07	0.08	0.08	*0.08*	*0.01*	0.13	0.10	0.12	*0.11*	*0.03*	0.89
Mn	0.01	0.01	0.01	*0.01*	*0.00*	0.01	0.00	0.00	*0.00*	*0.00*	0.01
Mg	1.89	1.91	1.91	*1.91*	*0.06*	0.86	0.89	0.88	*0.89*	*0.03*	0.12
Zn	--	--	--	--	--	0.00	0.00	0.00	*0.00*	*0.00*	0.00
Ca	0.00	0.00	0.00	*0.00*	*0.00*	--	--	--	--	--	--
TOTAL	2.99	3.00	3.00	*3.00*	*0.03*	3.00	3.00	3.00	3.00	*0.00*	3.00
X_{Mg}	0.96	0.96	0.96	*0.96*	*0.01*	0.87	0.90	0.88	*0.89*	*0.03*	0.12
X_{Mag}	--	--	--	--	--	0.08	0.04	0.03	*0.05*	*0.03*	0.99
activity	--	--	0.94	*0.94*	--	--	--	0.83	*0.83*	--	

*Fe_2O_3 and Fe^{+3} is recalculated after the scheme of Grew (2013) for spinel and magnetite Hc 0.15

X_{Mg} $=Mg/(Mg+Fe^{+2})$

X_{Mag} $=Fe^{+3}/(Fe^{+3}+Al^{+3})$

87^{TM} : Data used for textural and thermodynamic modelling

Clinohumite: $n(M_2SiO_4).M_{1-x}Ti_x(OH,F)_{2-2x}O_{2x}$ *:[n=4]*

Stoichiometry[A] = 2Si/[MTi*2n/(2n+1)]

M_{Ti}[B] = M + Ti :[M= Mg+Fe+Mn+Ca]

OH[C] =(2/2n+1)M-2Ti-F

:4)

SR78	*Average*		Sample	SR78	SR78	SR79	SR79	SR141	SR141	*Averag*
Mag	*Mag*		Mineral	Chu	Chu	Chu	Chu	Chu	Chu	*Chu*
36	*n=10*	*±2σ*	Point	92	107[TM]	95	3	5	74	*n=32*
0.01	*0.04*	*0.18*	SiO_2	37.58	38.05	37.93	38.84	38.82	37.98	*38.13*
0.61	*0.36*	*0.56*	TiO_2	2.88	1.22	2.80	1.97	1.87	1.14	*1.72*
0.48	*0.76*	*1.39*	Al_2O_3	b.d.l.	b.d.l.	b.d.l.	b.d.l.	b.d.l.	b.d.l.	*0.00*
0.06	*0.07*	*0.11*	Cr_2O_3	b.d.l.	b.d.l.	b.d.l.	b.d.l.	b.d.l.	b.d.l.	*0.00*
67.39	*66.83*	*2.50*	FeO	3.10	3.44	3.20	2.90	3.04	2.80	*3.18*
27.71	*28.19*	*2.27*	MnO	0.53	0.18	0.32	0.30	0.33	0.22	*0.29*
0.44	*0.46*	*0.49*	MgO	53.28	53.91	52.83	53.20	53.44	52.96	*53.15*
2.06	*1.52*	*1.72*	CaO	0.01	b.d.l.	0.03	0.05	b.d.l.	0.02	*0.02*
b.d.l.	b.d.l.	--	Na_2O	b.d.l.	0.01	0.02	b.d.l.	0.01	b.d.l.	*0.01*
--	--	--	K_2O	b.d.l.	0.02	b.d.l.	b.d.l.	b.d.l.	0.01	*b.d.l.*
98.77	*98.27*	*1.85*	F	1.14	1.37	0.96	1.50	1.15	1.83	*1.27*
4	--	--	Cl	b.d.l.	0.02	b.d.l.	0.01	0.01	0.01	*0.01*
0.00	*0.00*	*0.01*	O=F	0.48	0.58	0.40	0.63	0.48	0.77	*0.53*
0.02	*0.01*	*0.02*	O=Cl	--	0.00	--	--	--	--	--
0.02	*0.03*	*0.06*	TOTAL	98.00	97.66	97.64	98.13	98.16	96.24	*97.27*
0.00	*0.00*	*0.00*	Cation basis	13	13	13	13	13	13	--
1.94	*1.94*	*0.06*	Si	4.00	4.04	4.05	4.13	4.11	4.10	*4.07*
0.89	*0.91*	*0.08*	Ti (=X)	0.23	0.10	0.22	0.16	0.15	0.09	*0.14*
0.01	*0.02*	*0.02*	Al	0.00	0.00	0.00	0.00	0.00	0.00	*0.00*
0.12	*0.09*	*0.10*	Cr	0.00	0.00	0.00	0.00	0.00	0.00	*0.00*
0.00	*0.00*	*0.00*	Fe^{+2}	0.28	0.31	0.29	0.26	0.27	0.25	*0.28*
--	--	--	Mn	0.05	0.02	0.03	0.03	0.03	0.02	*0.03*
3.00	*3.00*	*0.00*	Mg	8.45	8.53	8.41	8.43	8.44	8.53	*8.47*
0.12	*0.09*	*0.10*	Ca	0.00	0.00	0.00	0.01	0.00	0.00	*0.00*
0.99	*0.98*	*0.03*	Na_2O	0.00	0.00	0.00	0.00	0.00	0.00	*0.00*
		--	K_2O	0.00	0.00	0.00	0.00	0.00	0.00	*0.00*
			TOTAL	13.00	13.00	13.00	13.00	13.00	13.00	*13.00*
			F	0.38	0.46	0.32	0.50	0.39	0.62	*0.43*
			Cl	0.00	0.00	0.00	0.00	0.00	0.00	*0.00*
			Stoichiometry[A]	1.00	1.02	1.02	1.05	1.04	1.04	*1.00*
			X_{Mg}	0.96	0.96	0.96	0.97	0.97	0.97	*0.97*
			X_F	0.19	0.23	0.16	0.26	0.20	0.32	*0.25*
			M_{Ti}/Si[B]	2.25	2.22	2.21	2.15	2.16	2.17	*2.25*
			OH[C]	1.16	1.34	1.23	1.18	1.31	1.19	*1.29*
			activity	0.11	0.07	0.12	0.07	0.08	0.06	*0.09*

ge

±2σ
1.24
1.16
0.03
0.02
0.41
0.19
1.44
0.07
0.05
0.03
0.51
0.02
0.22
--
2.38
--
0.09
0.09
0.00
0.00
0.04
0.02
0.11
0.01
0.01
0.00
0.00
0.17
0.00
0.07
0.02
0.11
0.16
0.18
0.04